Supporting Information

The enhancement of electron transportation and photo-catalytic activity for hydrogen generation by introducing spin-polarized current into dye-sensitized photo-catalyst

State Key Laboratory for Oxo Synthesis and Selective Oxidation, Lanzhou Institute of Chemical Physics, Chinese Academy of Sciences, Lanzhou, 730000, China.

College of Material Engineering, Jinling Institute of technology, Nanjing, China

*Corresponding author: E-mail: gxlu@lzb.ac.cn

1. Experimental section

1.1 Preparation of RGO-Pt and I-RGO-Ptcatalysts

(1) RGO-Pt catalysts

The RGO-Pt catalyst was synthesized by decorating the RGO sheets with Pt catalysts. In a typical synthetic process, 3 mL of graphene suspensions (3 mg/mL) was dispersed into 80mL TEOA-H_2O solution (v/v=10%, pH=11) under magnetic stirring. Then 70 mg Eosin Y as well as 1 mL aqueous K_2PtCl_6 (5mg/mL) were added into above solution. After magnetic stirring for 30 min, the mixed solution was degassed by bubbling Ar gas for 40 min. Then the photo-catalytic reaction and characterization of RGO@Pt catalysts were the same with that of Pt catalysts.

(2)I-RGO-Pt catalysts

I-RGO-Pt catalysts were the RGO-Pt catalysts decorated with different contents of Iodide elements. **Tab.S1** gives the detail about the atom ration of carbon and Iodide atoms (I/C) in different photo-catalysts. In a typical synthetic process, 3 mL graphene suspension (RGO, 3 mg/mL) was dispersed into 10 mL distilled water. Then, 0.5 mL PAAS (polyacrylate sodium) solution ($2*10^{-3}$ g/mL) was mixed into the above-prepared solution under magnetic stirring. Then 20μL$AgNO_3$ solution was mixed into above solution by ultrasonic vibration. After 30 min, 20μLKI solution were mixed into above solution and reacted with above solution under ultrasonic vibration for 30min.

The mixed solution was dispersed into 100mL triethanolamine (TEOA)-H_2O solution (v/v=10%, pH=11) under magnetic stirring. Then 70 mg Eosin Y as well as 1 mLK_2PtCl solution (5mg/mL) were added into above solution. After magnetic stirring for 30 min, the mixtures were degassed by bubbling Ar gas for 40 min. The photo-catalytic synthesis and characterizations of RPAI catalysts were the same with that of Pt catalysts.

Tab.S1 The reagents ratio of **RGO-Pt**, and **I-RGO-Pt** with different I/C ratio

I/C ratio	**RGO (1 mg/mL)**	**PAAS ($2*10^{-3}$ g/mL)**	**$AgNO_3$ (0.1 mol/L)**	**KI (0.1 mol/L)**	**K_2PtCl_6 (5mg/mL)**
0 (RGO-Pt)	3 mL	0.5 mL	0 μL	0 μL	1mL
0.02	3 mL	0.5 mL	20 μL	20 μL	1mL
0.05	3 mL	0.5 mL	50 μL	50 μL	1mL
0.1	3 mL	0.5 mL	100 μL	100 μL	1mL
0.2	3 mL	0.5 mL	200 μL	200 μL	1mL
0.3	3 mL	0.5 mL	300 μL	300 μL	1mL
0.5	3 mL	0.5 mL	500 μL	500 μL	1mL
1	3 mL	0.5 mL	1000μL	1000μL	1mL
1.5	3 mL	0.5 mL	1500 μL	1500 μL	1mL
2	3 mL	0.5 mL	2000 μL	2000 μL	1mL
2.5	3 mL	0.5 mL	2500 μL	2500 μL	1mL
3	3 mL	0.5 mL	3000 μL	3000 μL	1mL

1.3Characterization Details

Transmission electron microscopy (TEM) and high-resolution TEM (HRTEM) were taken with a Tecnai-G2-F30 field emission transmission electron microscope operating at an accelerating voltage of 300 kV. X-ray diffraction (XRD) patterns of the samples were recorded on a Rigaku B/Max-RB diffractometer with a nickel filtrated Cu Kα radiation operated at 40 kV and 40mA. X-ray photoelectron spectroscopy (XPS) analysis was performed using a VG Scientific ESCALAB210-XPS photoelectron spectrometer with an Mg Kα X-ray resource. Raman spectra were performed in air by high-resolution confocal μ-Raman system (Horiba JY, LabRam HR800).

EPR measurements were carried out on a Bruker EMX-8 and JEOL JES-TE200 X-band EPR spectrometers equipped with Oxford Instrument ESR900 and ESR910 cryostats, at PMW ranging from 2 μW to 200 mW. For EPR study the samples (each of ~5 mg) were sealed in a quartz capillary tube with 1 mm internal diameter and 50 mm length.

The amount of hydrogen evolution was characterized by gas chromatograph (Aglient 6820, TCD, 13×column, Ar carrier). The electrochemical measurements were measured on an electrochemical analyzer (CHI660A) in a standard three-electrode cell. Platinum foil was used as the counter electrode and a saturated calomel electrode (SCE) as the reference electrode. The working electrodes were prepared by drop-coating sample suspensions directly onto the precleaned glassy carbon electrode (GCE) surface (The sample prepared by the above method were dispersed in 2 mL of alcohol, and 40 μL of suspensions was coated on the surface of GCE).

The fluorescence decay time were measured using the Horiba Jobin Yvon Data Station HUB operating in time-correlated single photon counting mode (TCSPC) with the time resolution of 200 ps. Nano LED diode emitting pulses at 460 nm with 1 MHz repetition rate was used as an excitation source. The polarization degree of EY emission was measured by Polarization Fluorescence spectra using FS5 Spectrofluorometer (Edinburgh Instruments). The polarization degree (P) could be calculated by equation (1), the fluorescence anisotropy (r) was calculated by equation (2), and the correction factor (G) was calculated by equation (3)[S1].

$$\mathrm{P} = \frac{I_{VV} - I_{VH} \times G}{I_{VV} + I_{VH} \times G} \quad (1)$$

$$\mathrm{r} = \frac{I_{VV} - I_{VH} \times G}{I_{VV} + 2I_{VH} \times G} \quad (2)$$

$$\mathrm{G} = \frac{I_{HV}}{I_{HH}} \quad (3)$$

where I represents the intensity of the fluorescence signal and the subscripts define the orientation H for horizontal and V for vertical of the excitation and emission polarizers, respectively. G is the grating factor of the fluorescence spectrophotometer, which is used to correct for the wavelength response to polarization of the emission optics and detectors.

2Results and discussion

2.1 Polarization degree (P) and fluorescence anisotropy (r) of photo-catalysts

Tab.S2 Polarization degree (P) and fluorescence anisotropy (r) of photo-catalysts

I/C (atom ratio)	$\mathbf{I_{VV}}$(*10^4)	$\mathbf{I_{VH}}$(*10^4)	$\mathbf{I_{HH}}$(*10^4)	$\mathbf{I_{HV}}$ (*10^4)	**P**	**r**
0	8.836	12.54	26.92	18.06	0.01980	0.01248
0.01	8.865	12.08	26.55	18.17	0.02847	0.01805
0.02	7.84	10.76	23.16	15.47	0.03514	0.02226
0.10	7.937	10.06	22.6	15.32	0.06210	0.03983

Tab. S2 shows the Fluorescence Polarization data of each photo-catalyst. The values of polarization degree and fluorescence anisotropy were calculated according to those data.

2.2 Decay lifetime of the photo-catalysts

Tab. S3 Decay parameters of EY in the presence ofPt, RGO@Pt, RPAI-A, RPAI-B and RPAI-C

I/C (atom ratio)	**Lifetime (ns)**	**Pre-exponential factors A**	**A**	χ^2
0.10	τ1=1.45; τ2=3.15	A1=0.0324; A2=0.0251	0.59	1.00
0.02	τ1=1.18; τ2=3.22	A1=0.0482; A2=0.0181	0.51	1.00
0.01	τ1=1.28; 2=2.80	A1=0.0538; A2=0.0130	0.54	1.00
0 (RGO-Pt)	τ1=0.954; τ2=1.71	A1=0.0672; A2=0.0131	0.45	1.00
EY	τ=1.23	0.0727	0.33	1.00

2.3 XPS spectra

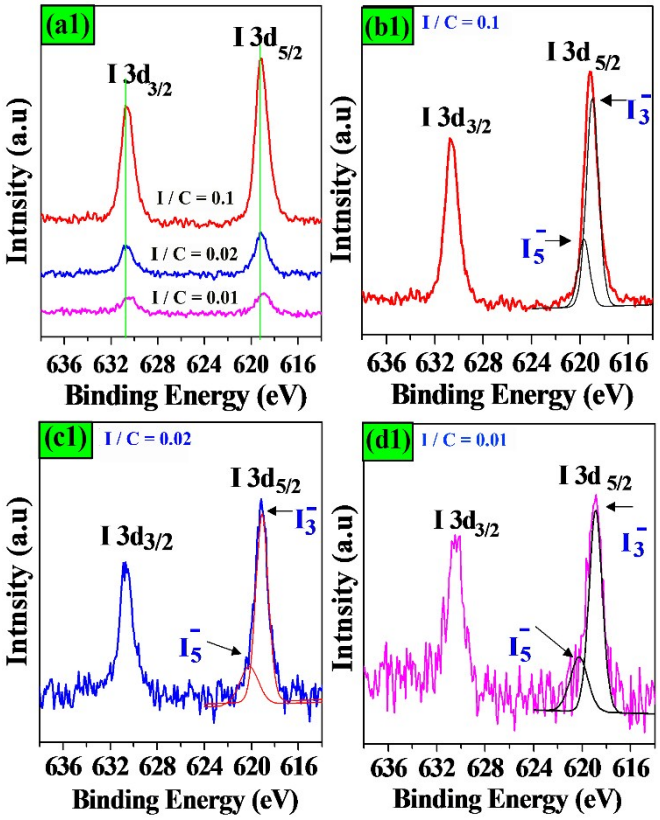

Fig. S1I 3d XPS spectra of I-RGO-Pt photo-catalysts (b1) I/C=0.1, (c1) I/C=0.02, (d1) I/C=0.01

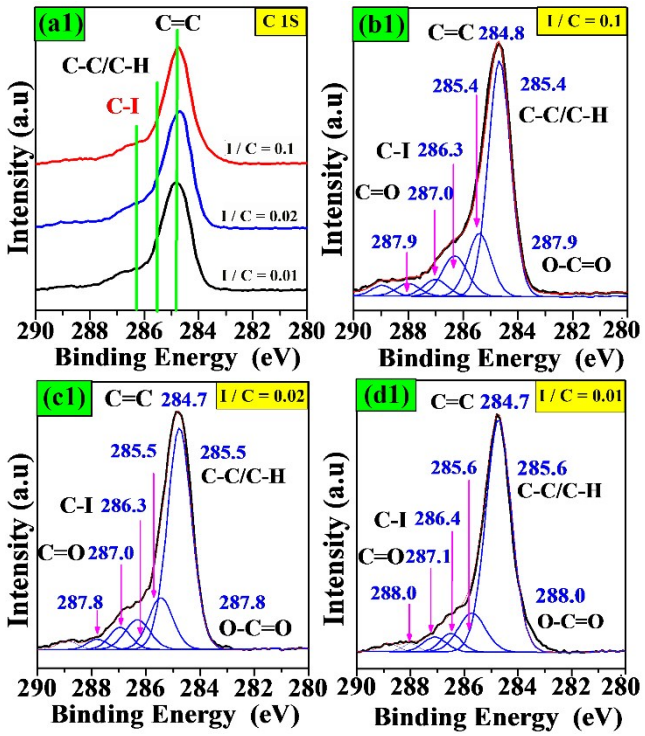

Fig. S2C 1s XPS spectra of I-RGO-Pt photo-catalysts (a2) I/C=0.1, (a3) I/C=0.02, (a4) I/C=0.01

2.4Raman spectra of the I-RGO-Pt photo-catalysts

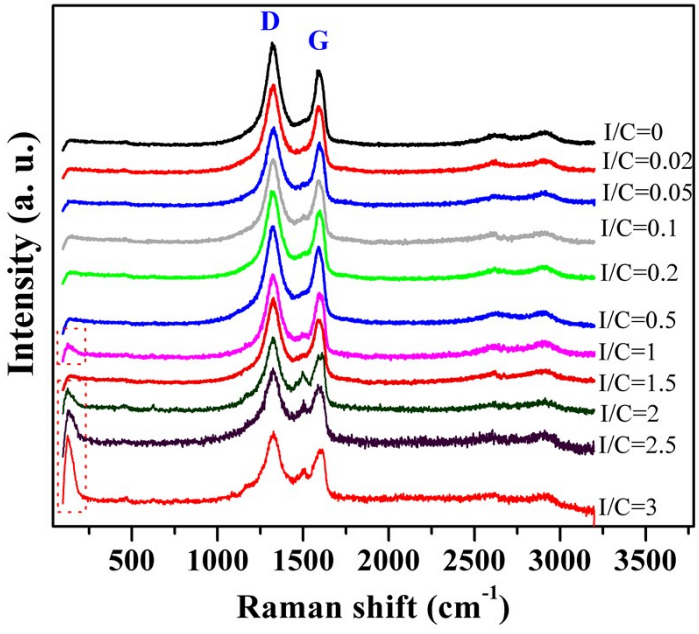

Fig. S3 Raman spectra of the I-RGO-Pt photo-catalysts with different I/C atom ratios

2.5 XRD patterns of the photo-catalysts

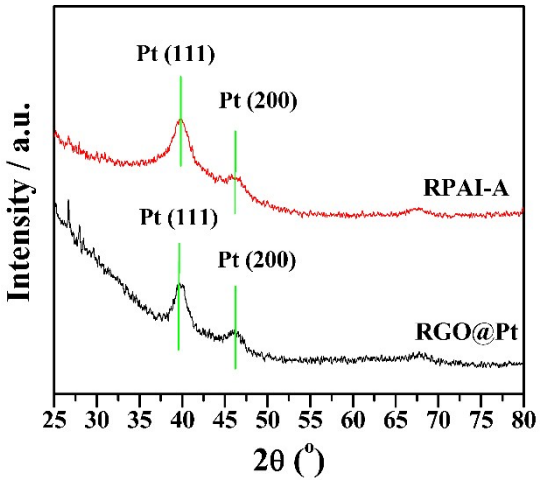

Fig. S4 XRD patterns of RGO-Pt and I-RGO-Pt catalyst (I/C = 0.1)

As shown in Fig. S4, XRD pattern of the RGO-Pt exhibits a strong and a weak diffraction peak, which could be assigned to the (111) and (200) planes of Pt. XRD pattern of I-RGO-Pt catalyst (I/C = 0.1) also exhibits a strong and a weak diffraction peak, whose positions are very close to the diffraction peaks of Pt. The two peaks could be assigned to the (111) and (200) planes of cubic Pt.

2.6 Recycle HER experiment over the I-RGO-Pt (I/C = 1) catalyst

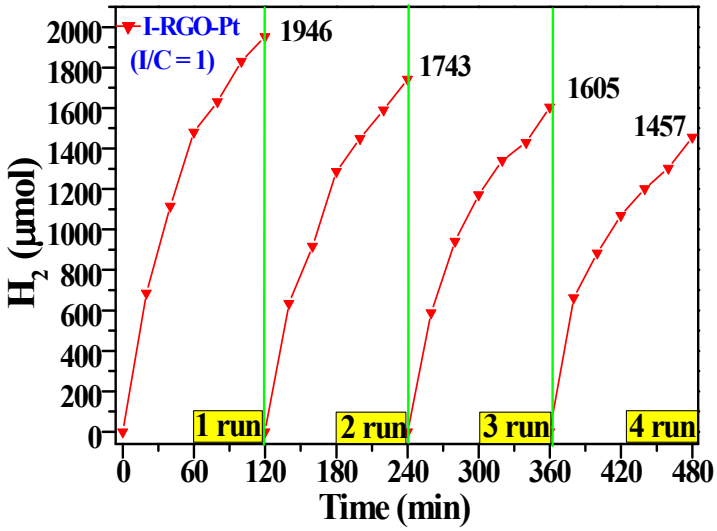

Fig. S5 Four recycles of HER over I-RGO-Pt I (I/C = 1) catalyst, sensitized by EY dye

Four recycles of HER were carried out over the I-RGO-Pt (I/C = 1) catalyst, as shown in Fig. S5. The HER system was sensitized by EY dye. The H_2 evolution remains 74.6% after four times recycling. The catalytic activity degradation could mainly be assigned the consumption of sacrificial donor [S17, S18]. In the HER reaction, tri-ethanolamine (TEOA) plays the role as sacrificial donor and the consumption of TEOA

could slow down the electron transfer between the EY and catalyst, as a result declining the photo-catalytic H_2 evolution activity of catalysts [S17, S18].

2.7 Details for the Hamiltonian of I-RGO

Firstly, we talk about the structure of RGO. The sp^2 hybridization of the 2s orbital and two 2p orbital of the carbon atoms create the σ bonds to form the honeycomb lattice of graphene, which is bipartite with two carbon atoms in one unit cell [S17]. The π band is consisting of the remaining 2p orbitals. The semimetal property of RGO is mainly ascribed to the contribution of 2p orbitals, as the states near the Fermi energy are π orbitals residing near the *K* and *K'* points at opposite corners of the hexagonal Brillouin zone [S8].

When the polyiodides are assembled on RGO to form I-RGO, their heavy atom effect will induce Rashba ***SOC*** on RGO, which could lead to the hopping and tunneling of electrons through the RGO. However, it should be noted that for RGO, only the ***SOC*** in the normal direction with the form $L_z\sigma_z$ has a non-zero contribution due to the reflection symmetry to the lattice plane [S17]. In other words, we suspect non spherical effects occurring in the geometry of RGO produce a crystal field that splits the energies of the p_z orbitals[17].

The Hamiltonian of the I-RGO can be written as[17,18,S8-S10]:

$H = H^R_{SO} + \delta H$

where H^R_{SO} corresponds to the Rashba ***SOC*** of flat RGO, and δH corresponds to the dependence of electrons' hopping energies on the contents of impurity, defects and sp^3 distortion in RGO.

The Rashba ***SOC*** on flat RGO could induces a coupling between first neighbors with opposite spin of the form[17,18]

$$H^R_{so} = i\lambda \sum_{<i_A,j_B>,\sigma,\sigma'} (\hat{\mu}_{i_A,j_B})_z \left| Z,i_A,\sigma >< Z,j_B,\sigma' \right|$$

$\hat{\mu}_{i_A,j_B}$ is a unit parallel vector, σ is the electron spin Pauli matrices, and $\left|Z,i_A,\sigma\right>$ represents the wave function of an electron occupying a carbon p_z orbital.

Now we consider the dependence of electrons' hopping energies δH, which includes a spin-orbit coupling part and a crystal field H_{CF} term[17].The Hamiltonian describing the electrons in the atom, contains

$$\delta H = \Delta_{so} \vec{L} \cdot \to \sigma + H_{CF}$$

where Δ_{so} is the spin-orbit coupling parameter, $\vec{L}$ and $\rightarrow\sigma$ are the usual angular momentum and spin operators. The $\vec{L}\cdot\rightarrow\sigma$ and H_{CF} can be written as

$$\vec{L}\cdot\rightarrow\sigma = 1/2\begin{bmatrix} 0 & -i & 0 & 0 & 0 & 1 \\ -i & 0 & 0 & 0 & 0 & -i \\ 0 & 0 & 0 & -1 & i & 0 \\ 0 & 0 & -1 & 0 & i & 0 \\ 0 & 0 & -i & -i & 0 & 0 \\ 1 & i & 0 & 0 & i & 0 \end{bmatrix} \quad (\{|p_x\uparrow>,|p_x\downarrow>,|p_y\uparrow>,|p_y\downarrow>,|p_z\uparrow>,|p_z\downarrow>\})$$

$$H_{CF} = \begin{bmatrix} \varepsilon_x & 0 & 0 & 0 & 0 & 0 \\ 0 & \varepsilon_y & 0 & 0 & 0 & 0 \\ 0 & 0 & \varepsilon_z & 0 & 0 & 0 \\ 0 & 0 & 0 & \varepsilon_x & 0 & 0 \\ 0 & 0 & 0 & 0 & \varepsilon_y & 0 \\ 0 & 0 & 0 & 0 & 0 & \varepsilon_z \end{bmatrix} \quad (\varepsilon_x = \varepsilon_y \neq \varepsilon_z)$$

When I/C atom ratio rose up to 1, there are large amounts of polyiodide (I^{3-} and I^{5-} clusters) on RGO. Those polyiodide have high charge density, which could induce irregular electric fields at the polyiodide's periphery. Such electric fields could be described as:

$$\vec{E} = \frac{1}{4\pi\varepsilon_0}\frac{Q}{r^2}\hat{r}$$

where $\vec{E}$ is the electric field, $\varepsilon_0 = 8.85\times10^{-12}\ \mathrm{C^2/(N\cdot m^2)}$ is the vacuum dielectric constant, r is the distance between the two charges, and $Q=1.602\times10^{-19}\mathrm{C}$ represents the point charge that is elementary charge. The existing of irregular electric fields could induce a large Rashba spin-orbit coupling and an idiosyncratic Hall conductivity in the randomly scattered I-RGO[17,S10]. The Hall conductivity could be written as:

$$\omega = \omega\uparrow + \omega\downarrow = 2\frac{e^2}{h}$$

where ω is the Hall conductivity of material, $\omega\uparrow$ and $\omega\downarrow$ represent different directions of the spin, and $h = 6.626\times10^{-34}\,J\cdot s$ is the Planck constant.

In our work, as the electron transfer enhanced in large scale, it is reasonable to attribute those improvement to the cross section for spin flip processes[17,S10].

2.8 Discussing about how the polyiodides ions deposited on the thin RGO nanosheet

As illustrated in Scheme S1, length of C-C bond is about 0.142 nm in the honeycomb lattice of ideal graphene. It could be calculated that the diameter (d_{AB}) of each hexagonal unit cell is about 0.284 nm. It could also be calculated that there are two carbon atoms in each hexagonal unit cell [S17]. As the diameters of I atom is 0.132 nm, there are enough space for the location of I atoms. Those I_3^- ions on RGO sheets mainly exist stably in linear chain structure [23].

In EY sensitized HER system, when C/I =1, the HER were promoted to maximum because the amounts of polyiodides on RGO reached an optimum value to induce large Rashba ***SOC*** effect on RGO. To analyze how the polyiodides ions deposited on the thin RGO nanosheet when C/I =1, it has to be considered that: (1) a RGO sheet has two sides; (2) there are two carbon atoms in each hexagonal unit cell. Based on those two considerations, it could be inferred that in ideal condition, on average, there is at least one I atoms deposited in each hexagonal unit cell if the polyiodides ions were assembled homogeneously on both side of the RGO sheets.

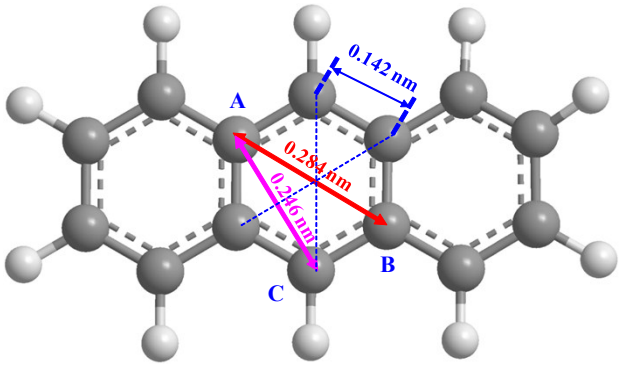

Scheme S1. Size of hexagonal unit cell in honeycomb lattice of ideal graphene

Reference

[S1] S. J. Zhen, Y. Yu, C. M. Li, C. Z. Huang, Analyst 2015, **140**, 353.

[S2] G. Kalita, K. Wakita, M. Takahashi, M. Umeno, J. Mater. Chem. 2011, **21**, 15209.

[S3] Y. F. Zhan, B. D. Zhang, L. M. Cao, X. X. Wu, Z. P. Lin, X. Yu, X. X. Zhang, D. R. Zeng, F. Y. Xie, W. H. Zhang, J. Chen, H. Meng, Carbon 2015, **94**, 1.

[S4] H. E. Lessing, A. V. Jena, M. Reichert, Chem. Phy. Lett. 1976, **42**, 218.

[S5] S. X Min, G. X. Lu, J. Phys. Chem. C 2011, **115**, 13938.

[S6] G. Kalita, K. Wakita, M. Takahashi, M. Umeno, J. Mater. Chem. 2011, **21**, 15209.

[S7] Y. F. Zhan, B. D. Zhang, L. M. Cao, X. X. Wu, Z. P. Lin, X. Yu, X. X. Zhang, D. R. Zeng, F. Y. Xie, W. H. Zhang, J. Chen, H. Meng, Carbon 2015, **94**, 1.

[S8] C. L. Kane, E. J. Mele, Phys. Rev. Lett. 2005, **95**, 226801.

[S9] Z. H. Qiao, W. K. Tse, H. Jiang, Y. G. Yao, Q. Niu,2011, Phys. Rev. Lett. **107**, 256801.

[S10] L. Brey, Phys. Rev. B 2015, **92**, 235444.

[S11] M. Tommasini, C. Castiglioni, G. Zerbi, A. Barbon, M. Brustolon, Chem. Phy. Lett. 2011, **516**, 220.

[S12] M. H. D. Guimarães, P. J. Zomer, J. Ingla-Aynés, J. C. Brant, N. Tombros, B. J. V. Wees, Phys. Rev. Lett. 2014, **113**, 086602.

[S13] L. Ciric, A. Sienkiewicz, D. M. Djokic, R. Smajda, A, Magrez, T. Kaspar, R. Nesper, L. Forro, Phys. Status Solidi B, 2010, **247**, 2958–2961.

[S14] L. Majchrzycki, M.A. Augustyniak-Jabokow, R. Strzelczyk, M. Mackowiak, ActaPhys. Polonica, 2015, **127**, 540.

[S15] S. Lijewski, M. Wencka, S. K. Hoffmann, M. Kempinski, W. Kempinski, M. Sliwinsk-Bartkowiak, Phys. Rev. B 2008, **77**, 014304.

[S16] S. Moulay, J. Polym. Eng., 2013, **33**, 389.

[S17] S. X. Min, G. X. Lu, J. Phys. Chem. C. 2011, **115**, 13938.

[S18] C, Kong, S. Min, G. X. Lu, Int. J. Hydrogen Energy 2014, **39**, 4836.